JULES-GL7: The Global Land Configuration of the Joint UK Land Environment Simulation version 7.0 and 7.2

r410

Andrew J. Wiltshire[1], Maria Carolina Duran Rojas[2], John M. Edwards[1], Nicola Gedney[1], Anna B. Harper[2], Andy Hartley[1], Margaret A. Hendry[1], Eddy Robertson[1], Kerry Smout-Day[1]

[1]Met Office, Fitzroy Road, Exeter. EX1 3PB. UK
[2]University of Exeter, Exeter, UK.

Correspondence to: Andrew J. Wiltshire (andy.wiltshire@metoffice.gov.uk)

Abstract.

We present the latest global land configuration of the Joint UK Land Environment Simulator (JULES) model as used in the latest international Coupled Model Intercomparison Project (CMIP6). The configuration is defined by the combination of switches, parameter values and ancillary data, which we provide alongside a set of historical forcing data that defines the experimental setup. The configurations provided are JULES-GL7.0, the base setup used in CMIP6 and JULES-GL7.2, a subversion that includes improvements to the representation of canopy radiation and interception. These configurations are recommended for all JULES applications focused on the exchange and state of heat, water and momentum at the land surface.

In addition, we provide a standardised modelling system that runs on the NERC JASMIN cluster, accessible to all JULES users. This is provided so that users can test and evaluate their own science against the standard configuration to promote community engagement in the development of land surface modelling capability through JULES. It is intended that JULES configurations should be independent of the underlying code base and thus they will be available at the latest release of the JULES code. This means that different code releases will produce scientifically comparable results for a given configuration version. Versioning is therefore determined by the configuration as opposed to the underlying code base.

1 Introduction

The Joint UK Land Environment Simulator (JULES) (Best et al., 2011; Clark et al., 2011) is the land surface model used by the UK land, hydrological, weather and climate communities. JULES is a comprehensive model simulating the atmospheric exchange of radiation, heat, water, momentum, carbon and methane and changes in the surface states of moisture, heat and carbon. All these processes are important for the wide ranging application of JULES from carbon cycle (Le Quéré et al., 2018) to climate impact (Shannon et al., 2018) and hydrological (Betts et al., 2018) modelling. However, each of these applications is best suited to a combination of different processes and schemes, for instance an interactive dynamic vegetation model is important to understanding carbon cycle processes but not crucial to crop modelling (Osborne et al., 2015) and may introduce additional biases and errors. The JULES code base enables a vast number of different setups through parameter and switch combinations, many of which are undesirable for a plethora of reasons from poor performance, lack of testing or incompatibility between options. This can lead to very poor scientific outcomes if the user is not completely familiar with the JULES code base. Addressing this is best achieved by having defined **science configurations**, specifying a particular combination of parameters and switches that are known to produce appropriate, well evaluated and tested results.

JULES is the land component of the Met Office modelling system, which is used across weather to climate timescales. Each component has defined configurations: the Global Atmosphere (GA) for configurations of the atmospheric model, Global Land (GL) configuration for JULES, and likewise for the ocean and sea-ice components, with the Global Coupled (GC) configuration for the fully coupled atmosphere, ocean, sea-ice and land model. Here, we present the JULES-GL7 configuration family developed primarily as part of the atmosphere model at the Met Office. JULES-GL7.0 is the offline version of the GL7.0 configuration used in conjunction with GA7.0 (Walters et al., 2017), the atmospheric configuration of the Met Office. These are the latest iterations in the GA/GL configuration series developed for use in global modelling and underpin the HadGEM3-GC3.1 (Williams et al., 2018) model that is being used as part of the sixth iteration of the Coupled Modelling Intercomparison Project (CMIP6) (Eyring et al., 2016). The GL7.0 configuration is specifically developed to simulate the exchange of heat, water and momentum generally known as the 'physical environment,' and therefore does not include biogeochemical components which come under 'earth system' modelling, neither does it include processes specifically related to climate impacts such as crops. It is the appropriate configuration for understanding hydrology and land surface processes relating to the partitioning of heat and radiation. In many ways, GL7.0 is the core JULES configuration as, for example, the earth system setup adds components to it to enable the simulation of the exchange of carbon and methane. We also describe a sub-version JULES-GL7.2 which includes an improved canopy radiation scheme and diffuse radiation effects. This version addresses some known issues in the treatment of radiative transfer through the canopy.

Although this is the first time a standalone standard configuration of JULES is being made available to the community, land configurations are widely established in weather and climate modelling. The predecessor to JULES was the Met Office Surface Exchange Scheme (MOSES, Cox et al., 1999). Configurations of MOSES2.2 (Essery et al., 2003) underpin the CMIP5 physical model, HadGEM2 (Martin et al., 2011) and the earth system model HadGEM2-ES (Collins et al., 2011). As of GL3 (Walters et al., 2011), configurations of JULES were introduced and have been developed over subsequent iterations of the model development cycle. The latest of which is GL7 as described here offline and as coupled to the atmosphere (Walters et al., 2017) and ocean (Williams et al., 2018). Future configurations are currently in development with the aim of reducing model biases and improving the representation of physical processes. For instance, GL8 will include updated snow process representation including a new scheme parameterising snow grain size growth (Taillandier et al., 2007) with the aim of reducing albedo biases over the Antarctic and Greenland ice sheets and GL9 to include improved spatially varying observationally based canopy height. Alternative examples of configurations have previously been made available to the community as a stop-gap measure but the provenance of these is unknown and has resulted in a number of cases of poor performance. The release of JULES-

GL7 is part of an activity to ensure integrity of science results and enhance future development and capability of JULES land surface modelling.

Here, we document the offline JULES-GL7 configurations and their release at JULES vn5.3. The release includes a standardised suite control setup to initialise, reconfigure, spinup and run a standard historical experiment. The release is designed to be as easy as possible to access and run on the NERC JASMIN platform (http://www.jasmin.ac.uk/). Further details on running the JULES-GL7 configurations are given in Appendix A. The provision of standard configurations is an important step in the ongoing aim for community development of configurations underpinning weather, climate, hydrological and impact modelling in the UK. Future developments will include improved benchmarking and evaluation tools.

1.2 JULES Configurations

Defining JULES configurations and how they should be used and developed is therefore an essential component of improving land surface modelling. At the core of an application is the science configuration, which is the collection of parameters, ancillaries and switches necessary to produce the same results for a given experimental setup. The experimental setup covers the necessary model forcing information to produce a simulation. For example, the setup provided here uses historical meteorological information to perform a simulation from the pre-industrial to present day at n96 (1.875º x1.25º) resolution. Alternative experimental setups may be running future scenarios such as those included in CMIP6 (Eyring et al., 2016). The third component provided here is a standardised way by which the science and experimental configuration can be setup and run and is largely provided to support ease of access and use by a diverse range of users. This done by way of a suite compatible with the Rose/Cylc suite control system (https://metomi.github.io/rose/doc/html/index.html) available on JASMIN. The control system orchestrates the flow of inter-dependent tasks (workflow) from the initial extraction of the source code from repository, subsequent build and installation of the science and experimental setups and finally controls the simulation on the compute platform. The suite is the collection of all the information to make a simulation from start to finish in a format compatible with the workflow manager and a user-friendly graphical user interface.

JULES is a configurable model in which a named set of values control the operation of the model. JULES as a code base can support a number of these value sets that define different configurations. An important concept in the development of JULES-GL configurations is the independence of configuration from code release. JULES is managed to ensure that new developments in the code base produce scientifically comparable results. This is not exactly the same as reproducible to the bit level as some changes are permitted for example technical changes to the code base that result in explainable bit level changes. From a user perspective the differences between model releases should be pragmatically indistinguishable for a given configuration. The easiest way to ensure this, is for new developments to be put onto a switch. JULES-GL7 will be available at subsequent model versions and tested to ensure the setup produces scientifically comparable results between model code base versions until a date when JULES-GL7 is superseded and retired. A second concept is that JULES as a code base can support multiple configurations dependent on the desired application. The two major configurations are Global Land and Earth System. The Earth System extends the Global Land to include biogeochemical processes important to understanding feedbacks in the climate system.

The ancillary data component or ancillaries of a configuration are the spatially explicit information that varies according to the site or from gridbox to gridbox in the case of a gridded run. An example of this would be landcover. In the case of a gridded experiment these data typically are derived from high resolution satellite or observation based sources, which have to be post-processed to meet the requirements of JULES. The exact ancillary data vary according to the experimental setup (i.e. resolution,

individual site, etc) but as far as possible the mechanism by which the JULES specific information is derived from the source data is part of the science configuration. In the case of landcover in GL7 this would include the aggregation of landcover types into surface tile types from IGBP maps (Section 2.1). Here, we include a description of the ancillary generation process and include the ancillaries for an n96 experimental configuration simulating the twentieth century.

The JULES suites and online resources are available via the Met Office Science Repository Service (MOSRS) (https://code.metoffice.gov.uk, login required) and are freely available subject to completion of a software licence (Appendix A). Living documentation of the latest suite version can be found here. (https://code.metoffice.gov.uk/trac/jules/wiki/JulesConfigurations, login required)

2 JULES-GL7 Configuration

This section describes the offline JULES-GL7.0 and JULES-GL7.2 science configurations. An important difference between the offline and coupled versions is that in the coupled version JULES acts as an interface between land (including land-ice), sea-ice and the ocean whilst offline only land is considered. Important parameters are listed in Tables 1 and 2, ancillaries in Table 3 and in most cases, switches are listed in the text. The full set of switch settings can be found in the Rose suites. We include the full parameter tables for the surface tiles here for clarity as the Rose suites namelists encompass all parameters in JULES many of which are linked to particular switches and options and therefore not used in JULES-GL7. Work is progressing to simplify the Rose suite namelists using existing tools within Rose to hide unused parameters and options. The appropriate JULES documentation papers remain Best et al. (2011) and Clark et al. (2011). Where new developments are included, they are described in more detail with appropriate references herein.

2.1 Surface Tiling

JULES-GL7 uses a surface tiling scheme to represent subgrid heterogeneity. Within a gridbox, each tile has its own surface energy budget and is coupled to a single shared soil column (Figure 1). Each tile therefore has its own albedo, surface conductance to moisture, turbulent fluxes, ground heat flux, radiative fluxes, canopy water content, snow mass and melt, and thus surface temperature. Each tile requires its own parameter set which are given in Tables 1 (non-vegetated surface types) and 2 (vegetated surface types) and spatially explicit parameters in Table 3.

There are nine surface tiles consisting of five Plant Functional Types (PFTs) (Broadleaf trees, Needleleaf trees, C3 grass, C4 grass, Shrubs) and four non-vegetated surface types (Urban, Inland Water, Bare Soil and Ice) (Figure 2). These can co-exist in the same gridbox except for ice. The C4 distinction reflects a different photosynthetic pathway with all other PFTs represented as C3. The tile fractions are spatially varying and are read from an ancillary file. The fractions are produced by a re-mapping of the 17 surface types in the International Geosphere-Biosphere Programme (Loveland and Belward, 1997) to the 9 surface types in JULES. The landcover class remapping procedure is described in Table 4 of Walters et al. (2018) and the cross-walking table relating land-cover classes to PFTs in Table B1.

2.1.1 Plant Functional Types (PFTs)

Vegetation is represented by the five plant functional types described above. In JULES-GL7 each PFT has its own energy budget including thermal heat capacity (*CanMod=4*), which is a function of the PFT height (Sections 2.1.1.1 and 2.3). Leaf level stomatal conductance and photosynthesis are coupled through CO_2 diffusion with PFT specific parameters controlling sensitivity to humidity deficit and internal to external CO_2 pressures (Cox et al., 1998 and Table 2; *f0, dqcrit*). This coupling

implies that both the energy and carbon cycles are closely related; rising atmospheric CO_2 influences stomatal conductance and therefore the surface energy budget. This mechanism is known as physiological forcing (Betts et al., 2007; Field et al., 1995; Sellers et al., 1996). Leaf level conductance must be scaled to the canopy level and in JULES-GL7 this is done using a 10 layered canopy approach (*CanRadMod =4*). At each level separate direct and diffuse Photosynthetically Available Radiation (PAR) levels are calculated using the two-stream approach (Sellars, 1985) to give a profile of PAR through the canopy. From this the leaf level photosynthesis can be calculated using PFT specific parameters combined with the Collatz (1992, 1991) leaf biochemistry model utilising separate mechanisms for C3 and C4 plants (Jogireddy et al., 2003; Mercado et al., 2007). At each level, if net photosynthesis is negative or stomatal conductance is below a minimal threshold (*glmin*, Table 1), the stomata are closed and the stomatal conductance is set to this minimum. A further mechanism scales leaf level conductance via photosynthesis according to the availability of soil moisture in the rooting profile. In JULES-GL7, this scalar (β) relates the rooting profile (*rootd,* Table 2) in each soil layer with the availability of soil moisture. β is a piecewise function that scales from 0 when soil moisture is at or below the *wilting point* to 1 where soil moisture is above the *critical point* (Eq 12; Best et al., 2011). The root fraction weighted (*fsmc_mod=0*) total across soil layers value of β is used to scale photosynthesis at the leaf level. Canopy conductance is the leaf area weighted sum of leaf conductance across the 10 levels. A direct output from this setup is a diagnostic of Gross Photosynthetic Potential (GPP). However, as this is the non-biogeochemical configuration the fixed GPP does alter the canopy structure.

2.1.1.1 Spatial Leaf Area and Canopy Height ancillary data

Leaf Area Index (LAI) is defined as the one-sided surface area of canopy leaf cover per unit area of land and is defined spatially and temporally for each vegetated surface tile in JULES-GL7. Similarly, canopy height is spatially varying per vegetated tile but fixed in time. The ancillaries are derived from satellite data processed to be consistent with the landcover and plant functional type classifications used in JULES-GL7. To do this requires decomposing a 'mixed' signal from the satellite data into individual PFT contributions. This is achieved via an additional parameter, the "balanced" LAI (*Lb*), meaning the LAI that would be reached if the plant was in full leaf (Table B2). The combination of the mapping from land cover classes to PFTs and the balanced LAI weighting per PFT per land cover class allows the observed gridded satellite value to be decomposed into individual PFT contributions.

In JULES-GL7, monthly variations in LAI about the balanced LAI are based on a climatology for the period 2005 to 2009 derived from the MODIS LAI product (MOD15; (Yang et al., 2006)). The LAI value for a given PFT, land cover class and month are calculated as follows:

$$LAI_{i,j} = LAI_{MODIS} \frac{(Lb_{i,j}\alpha_{i,j})}{\sum_i (Lb_{i,j}\alpha_{i,j})}$$

Equation 1

Where LAI_i is the LAI for PFT class i, LAI_{MODIS} is the MODIS LAI value for a given month, $Lb_{i,j}$ is given by the LAI lookup table (Table B2), $\alpha_{i,j}$ is the fraction of each PFT i in IGBP class j given by the lookup table in Table B1. The PFT-specific LAI (LAI_i) is accumulated for all land cover classes in a gridbox for a given month. The resulting input ancillary is then internally interpolated within JULES to each model timestep. The seasonally-varying LAI for 5 PFTs for 30-60°N is shown in Figure 3. An outcome of this approach is that JULES is forced with the snow-free LAI which explains the large winter reductions in LAI for needleleaf trees. Improving the treatment of LAI in the ancillary information is a priority development for future versions of GL.

The introduced balanced LAI has the property of being allometrically related to the canopy height. Based on this allometric relationship the canopy height (*H*) can be derived for each PFT in each landcover class (Jones, 1998):

$$H_{i,j} = h_i Lb_{i,j}^{\frac{2}{3}}$$

Equation 2

Where h_i is a PFT specific scalar given in Appendix B (Table B3). The PFT cover mean height (*canht*) is the area weighted arithmetic mean of the landcover classes in that gridbox. Canopy height (Figure 4) is therefore based on allometric scaling of landcover class dependent parameters. Improving the representation of canopy height is also a priority area for future developments.

2.1.2 Non-vegetated surface types

The four non-vegetated surface types (urban, inland water, bare soil and land ice) like the vegetated surface types are represented as tiles with separate energy balances, described using the parameters listed in Table 1. A full description of the representation of the non-vegetated surface types can be found in Best et al. (2011) and the developments since this paper have been highlighted here. Since GL3.0 (Walters, et al., 2011) the urban surface has been represented by the simple one-tile scheme (*l_urban2t=.false.*), which consists of a radiatively coupled (*vf*, Table 1) "urban canopy" with the thermal characteristics (*ch*, Table 1) of concrete (Best, 2005). The urban canopy has a capacity to hold water (*catch*, Table 1) and when wet the surface moisture resistance is reduced to zero. Similar to the urban surface, lakes are represented as a radiatively coupled "inland water canopy" with the thermal characteristics of a mixed layer depth of water ($\approx$ 5m). The original representation of inland water, as a freely evaporating soil surface (*ch* = *vf* = 0.0, Table 1), was shown to have incorrect seasonal and diurnal cycles for surface temperatures and therefore evaporation (Rooney and Jones, 2010). The high thermal inertia of the urban and lake tiles results in an improved diurnal cycle in surface air temperature. Bare soil or bare-ground surface types are represented as having no canopy heat capacity and a surface moisture resistance to evaporation as a function of surface soil moisture (Eq 17, Best et al., 2011). Ice surfaces are an exception to the representation of surface heterogeneity as only ice can exist in a gridbox. This is because the sub-surface is modified to represent the thermal characteristics of ice. No infiltration is allowed, and all melt is assumed to be surface runoff. The surface temperature is limited to the melting point with the residual energy balance term assumed to be melt. As such ice surfaces do not conserve water.

The roughness lengths for inland water, bare soil & ice were updated to their current values as part of GL4.0 (Walters, et al., 2014). The roughness length (*z0* – Table 1) for inland water was reduced to 1×10^{-4} m as GL3.0 suffered from a slow bias when compared to reanalyses in the near-surface wind speed around the Great Lakes. This reduced value is more consistent with the values predicted from wind-speed-dependent parametrisations over open water (Walters, et al., 2014). The roughness length for bare soil was increased to 1×10^{-3} m, an intermediate value between those used in GL3.0 (3×10^{-4} m) and GL3.1 (3.2×10^{-3} m, used in operational global NWP forecasting). Observational estimates of the roughness length of bare soil surfaces suggest large geographical variations covering this range. The ratios of the roughness lengths for heat to momentum *(z0hm* – Table 1) were also revised as part of GL4.0 in conjunction with the roughness length changes. From GL4.0 the urban surface has used the Best (2006) value of 1×10^{-7} m; for inland water, the ratio has been set to 0.25 consistent with the parameterisation for open sea; bare soil was decreased to 0.02 to address a significant underestimate of the near-surface temperature gradient over arid regions; and ice was adjusted to 0.2 to be consistent with sea-ice. Prior to GL4.0, all ratios had a fixed value of 0.1. Another new capability introduced with GL4.0 was an emissivity for each surface type (*emis* – Table 1) based on the data of (Snyder, Wan, Zhang, & Feng, 1998) and additionally for bare soil, satellite retrievals of land surface temperature from over the Sahara. Previously these values were fixed at 0.97 regardless of surface type. The significant reduction in the bare soil emissivity improved a cold bias over the Middle Eastern deserts that was

prominent in GL3.0. The description of the non-vegetated surface types in JULES-GL7 remains largely unchanged since GL4.0 (Best et al., 2011).

2.2 Radiation

Typically, standalone JULES is driven with downward short wave and long wave radiative fluxes. To obtain the net fluxes that enter the surface energy budget, the surface albedo and emissivity must be calculated. The albedo varies with wavelength, although, for many natural surfaces, it is adequate to distinguish between the visible and near infrared parts of the spectrum. In reality, the albedo is also different for direct and diffuse radiation, but a distinction is not made for every surface in GL7.

For unvegetated surfaces single broadband albedos are used (*albsnf*, Table 1). The albedo of bare soil must be specified as ancillary data, but fixed values are used for the other three unvegetated tiles.

The albedo of plant canopies is calculated using the two-stream radiation scheme described by Sellers (1985). As inputs, this requires separate transmission (*omega, omnir*, Table 2) and reflection coefficients (*alpar, alnir,* Table 2) in the visible and near infrared regions respectively for individual leaves (or shoots in the case of needleleaf trees) and the leaf area index. It returns the visible and near infrared albedos for direct and diffuse radiation. However, the direct components are discarded and not used in GL7 for reasons of performance when coupled to the UM. When coupled to the UM, there is an option *(l_albedo_obs)* to scale the leaf-level characteristics to match a specified climatology of the albedo, but this unavailable offline.

A new albedo scheme for snow-covered surfaces was introduced into GL7. This incorporates a two-stream algorithm for the snow pack. The surface is modelled as an underlying soil surface, above which there is a plant canopy that is gradually buried as snow accumulates. The canopy is therefore modelled as a lower snow layer and an upper layer of exposed vegetation that will be absent if the snow is deep enough. The scheme makes explicit use of the canopy height. If canopy snow is allowed on the tile, there will also be a layer of snow on the canopy that is treated using the same two-stream scheme. Additional parameters (*can_clump, n_lai_exposed*) represent the vertical distribution of leaf-area density and the clumping of snow on the canopy. However, the values adopted in GL7 have been tuned to work with the existing ancillaries of canopy height which exhibit unrealistically limited spatial variability. Previously, a hard-wired lower limit of 0.5 had been imposed on the LAI in the calculation of the albedo. At GL7 this has been removed and replaced with separate limits for snow and snow-free conditions. In snow-free conditions, the nominal lower limit has been set to 0.005, while in the presence of snow a limit of 1.0 is imposed for trees and a limit of 0.1 in the case of short vegetation (Table 2). Infrared emissivities are specified as single broadband values for each surface type (Tables 1 and 2).

2.2.1 Diffuse Radiation

GL7 assumes that photosynthetically active radiation (PAR) is half of total downwelling shortwave. The PAR as seen in the plant physiology is entirely direct, which results in a lower penetration of PAR into the canopy and reduced photosynthesis at the sub-canopy level. For GL7.2 we introduce a constant global mean diffuse fraction of 0.4, based on output from the SOCRATES radiative transfer scheme (Edwards & Slingo, 1996; Manners et al., 2015). This has the impact of increasing light penetration into the canopy and therefore increasing GPP. To further improve GPP, we updated the canopy radiation model (*can_rad_mod*, changed from 4 to 6). Like *can_rad_mod*=5, 6 introduces sunfleck penetration through the canopy ($fsun = \exp(-\frac{k_b}{\cos z} LAI); k_b \ constant \ value \ of \ 0.5$) which increases the light within the canopy particularly for high solar zenith angles. Furthermore, *can_rad_mod=6* introduces a new nitrogen profile through the canopy following $\exp(-k_{nl}LAI)$, where k_{nl} is a PFT constant of 0.2 (Table 2). This has the effect of increasing potential GPP in canopies with low LAI (< 5) and

decreasing at high LAI (>5). GL7.2 is consequently a physically more realistic configuration of JULES. The changes to canopy radiation do not affect the simulated albedo as in the current setup the albedo is only calculated for direct radiation. GL7.0 and 7.2 will therefore have the same albedo, but the way light interacts with the canopy differs and therefore affects the exchange of moisture and carbon.

2.3 Surface Exchange

The representation of the surface energy budget in JULES is described by Best et al. (2011). The scheme includes a surface heat capacity. Atmospheric resistances are calculated using standard Monin-Obukhov surface layer similarity theory, using the stability functions of Beljaars and Holtslag (1991). Evaporation from bare soil and water on the canopy and transpiration through the plant canopy contribute to the latent heat fluxes. In the case of needle-leaved trees, snow on and beneath the canopy is treated separately (*can_mod=4*).

2.4 Soil Hydrology and Thermodynamics

Soil processes are represented using a 4-layer scheme for the heat and water fluxes with hydraulic relationships taken from van Genuchten (1980). The four layers (0.1, 0.25, 0.65 and 2m) are chosen to capture diurnal, seasonal and multiannual variability in soil moisture and heat fluxes. The JULES-GL7 soil parameter values are based in part on those developed for the MOSES model by Dharssi et al., (2009) and Cox et al., (1999) and are read from an ancillary. There is an additional deep layer with impeded drainage to represent shallow groundwater thus enabling a saturated zone and water table to form. The sub-grid scale soil moisture heterogeneity model is driven by the statistical distribution of topography within the grid box, and is based on a TOPMODEL-type approach (Gedney et al., 2003). The baseflow out of the model is dependent on the predicted grid box mean water table while surface saturation and wetland fractions are dependent on the distribution of water table depth within the grid box. The scheme uses the Marthews et al., (2015) topographic index dataset at 15 arc-sec resolution, which in turn is derived from HydroSHEDS (Lehner et al., 2006). The soil and hydrological ancillaries required are listed in Table 3.

2.5 Snow

A major difference between GL7 and earlier GL configurations is the activation of the multilayer snow scheme in JULES that is described by Best et al. (2011). This replaces the previous so-called zero-layer scheme in which a single thermal store was used for snow and the first soil level, and an insulating factor was applied to represent the lower thermal conductivity of snow. The zero-layer scheme included no representation of the evolution of the snow pack. Compared to the version described in Best et al. (2011), a number of enhancements have been introduced into the multilayer scheme in order to better to represent the thermal state of the snow surface and atmospheric boundary layer when coupled to the UM. The changes are noted in the following description and parameter values in Table 2.

In the multilayer scheme, the snow pack is divided into a number of layers, that are added or removed as the snowpack grows or shrinks. A maximum of 3 layers is imposed in GL7. In a deep snow pack, the top layer will be 0.04 m thick, the second 0.12 m thick, while the lowest layer will contain the remainder of the snow pack. Very thin layers of snow (less than 0.04 m deep) are still represented using the zero-layer scheme for reasons of numerical stability. The thickness, frozen and liquid water contents, temperature and grain size of each layer are prognostics of the scheme. New snow is added to the top of the snow pack and compaction by the overburden is included. Following these operations, the snow pack is relayered to the specified thickness.

The density of fresh snow has been set to 109 kg m^{-2}, following the scheme adopted in the CROCUS model (Vionnet et al., 2012), but omitting the wind-speed and temperature-dependent factors. The conductivity of snow was originally calculated using the parameterization of Yen (1981), but this has been replaced with the scheme proposed by Calonne et al. (2011). This gives higher conductivities in snow of low density, thereby strengthening the coupling between the snow pack and the boundary layer.

Again, with a view to improving the coupling between the atmosphere and the snow pack, the parameterization of equitemperature metamorphism described by Dutra et al. (2010) has been introduced. This accelerates the rate of densification of fresh snow and is important in reducing cold biases that would otherwise result.

In the original scheme, when the canopy snow model was selected, unloading of snow from the canopy occurred only when it was melting. In GL7, unloading (*unload_rate_u*, Table 2) is also permitted at colder temperatures and the timescale is set to 1/(2.31e-6*U10), which is tuned to give an unloading timescale of 2 days in the Canadian boreal forest in winter (MacKay and Bartlett, 2006) for the average 10 m wind speed predicted in the UM. Note that a separate canopy is currently used only for the needleleaf tile.

Unlike the original scheme, where it simply bypassed the snow pack, rain water is now allowed to infiltrate. Below a canopy, this infiltrating water includes melting from the canopy.

2.6 Coupled versus Uncoupled Differences

JULES has been developed in more than one modelling environment i.e. standalone and coupled with the UM, and consequently some science options are not available under all environments. This could be because certain science options only make sense in a coupled environment or the converse may be true. This is not true for all options and in some cases the options have only been implemented in one environment and require additional coding to make it available to others. Other differences arise out of the method of coupling the available driving data. When coupled, the surface meteorological state is solved interactively whereas offline this is provided either from observation or reanalysis products. One important difference concerning the treatment of radiation (*jules_radiation*) is that when coupled separate radiative fluxes of NIR and PAR are available from the radiation scheme however, offline typically only broadband shortwave is available and it is assumed this can be split 50:50 between NIR and PAR. Furthermore, when coupled, snow-free albedos on each surface type are nudged towards an observed climatological mean from an ancillary (*l_albedo_obs* = .*true*.). This approach maintains sensible differences between surface types and allows spatial differences in albedo properties to be captured, while agreeing well with observations. However, in turn this has some limitations and as such it is not suitable for climate change experiments that include a change in land cover. It is therefore not compatible with the dynamic vegetation and land-use models as used in the interactive carbon cycle option and thus is not implemented in the offline JULES-GL7 configuration. Another subtle difference concerning the treatment of radiation is the calculation of the solar zenith angle. When coupled, the SOCRATES radiative transfer scheme calculates this, whereas in standalone JULES the solar zenith angle calculation needs to be explicitly turned on using *l_cosz* = .*true*. to be equivalent. When using JULES-GL7 therefore with site data, care should be taken to ensure that the model and forcing data is in Coordinated Universal Time (UTC), as time is used in the calculation of solar zenith angle.

There are several differences in the treatment of the JULES surface exchange (*jules_surface*) as this is the interface between the surface and either the driving model or the driving data. Orographic form drag (*formdrag = 0 standalone, 1 coupled*) for example cannot be used in the standalone configuration as the necessary ancillary data is not available to standalone. In any

case, it may not make scientific sense to include as the orographic drag may be implicit in the driving data whether from observations or from model generated driving data. The method of discretization in the surface layer is another difference between the two environments, which affects how the driving data is interpreted. The driving data, when standalone, is most likely to be at a specific level (*i_modiscopt = 0*) rather than a vertical average as it is when coupled (*i_modiscopt = 1*). Also in the coupled model, a parametrisation of transitional decoupling in very light winds is included in the calculation of the 1.5 m temperature (*iscrntdiag =2*), however in standalone the surface is driven by the temperature at 1.5 m and is therefore is not a diagnostic. It is not recommended that the surface is driven with a decoupled variable as this scenario has not been properly tested and should instead be *iscrntdiag = 0*. And finally concerning the surface exchange, the coupled model includes the effects of both boundary layer and deep convective gustiness (*isrfexcnvgust = 1*), however this is not appropriate in standalone and therefore *isrfexcnvgust = 0*. When driving standalone JULES with observations at a high enough frequency the gusts would be implicit in the observational data; and in the case of driving JULES with a longer-term average, where there may be a gust contribution, the relevant information is not accessible.

3 JULES-GL7 Experimental Setup and Suite Control

The science configuration consists of a defined set of parameters and switches that can be used in conjunction with an experimental setup. The experimental setup differs from the configuration as it describes the conditions under which the configuration is applied. For example, in this case the setup is a global historical experiment, but it could also be a future climate scenario, driven by alternative historical forcing or at a multiple locations such as FluxNet sites, where more detailed evaluation data are available (e.g. Harper et al., 2016). The experiment in the suite provided is a global historical run from pre-industrial (1860) to present day (2014) including rising atmospheric CO_2 but fixed landcover. This is a standard historical experimental setup as used in the Global Carbon Project (Le Quéré et al., 2015). The climate data (CRU-NCEP v7) consists of 6-hourly NCEP data corrected to CRU climatology and observations updated to 2014 (CRU TS3.23; Harris et al., 2015). The original data were provided on a $0.5° \times 0.5°$ grid and subsequently regridded to a coarser resolution for consistency with the standard resolution climate experiments for CMIP6 using HadGEM3-GC3.1 at $1.875° \times 1.25°$. The forcing data include both gridded observations of climate and global atmospheric CO_2, which change over time (Dlugokencky and Tans, 2015). However, the CRU-NCEP data only start in 1901. To begin the experiments in 1860, a time when atmospheric CO_2 was relatively stable, requires the years 1901-1920 to be replicated between 1860 and 1900 thus assuming no effect of climate change between 1860 and 1901. CRU-NCEP uses a 365-day calendar so no leap years are included. Furthermore, CRU-NCEP is a land-only dataset including Greenland but excluding Antarctica. At the coarser resolution, a gridbox may only be partially land-covered. JULES works on the land only fraction of the gridbox. It is therefore important when making global means or averages that both the land fraction of a gridbox as well as the gridbox area is considered. An important provided ancillary is therefore the land fraction (Table 3).

The suite as provided, includes a standardised suite control approach to manage both the necessary stages of initialising and running an experiment, as well as scheduling resources and timeslots on the supercomputer. This is shown graphically in Figure 5. The suite is set up to run three separate instances of JULES. The first initialises and reconfigures an initial start condition. The second starts from the reconfigured start condition and spins up the states of snow, soil moisture and temperatures by cycling over 1860-1879 climate using fixed pre-industrial CO_2. This is optional according to whether the initial state is already spun-up and is controlled by a switch (*l_spinup)*. Setting this switch to false bypasses spinup entirely. The number of cycles required and the period to loop over can also be set. Each new cycle of spinup is submitted as a new job taking the initial conditions from the end of the previous cycle. The final task is to perform the transient experiment taking either initial conditions from the reconfiguration step or the final spinup cycle. These settings are all available under *Runtime*

Configuration and *Runtime Configuration > Spinup Options.* The transient run makes uses of varying climate and atmospheric CO_2. As standard the transient experiment has a 10 year cycle interval to allow a complete cycle to complete within the time limits on the supercomputer. It is worth noting that JULES vn5.3 is unable to perform full bit comparable restarts. This means the model prognostics at the end of one submission differ slightly from those used at the start of the next. The exact state at the end of the transient run will therefore be dependent on the number of spinup and transient cycles used.

4 JULES-GL7 Evaluation

In this section we evaluate the CRU-NCEPv7 historical experimental setup of the JULES-GL7 model configuration. We follow the approach of the International Land Model Benchmarking (ILAMB) project tool (Collier et al, 2018) to compare model simulations against observational data. However, due to technical limitations we are unable to use the full benchmarking range that ILAMB includes. Here, we assess model performance against three key metrics covering surface energy balance, hydrology and vegetation productivity. The metrics are annual mean albedo, evapotranspiration and gross primary productivity and they are benchmarked against observationally based datasets available in ILAMB. The aim here is not to perform a full analysis of model skill but to establish a few important benchmarks against which model developments can be compared and evaluated. In time, it is planned that the standardised JULES suite will be fully compatible with ILAMB allowing for a full model evaluation and benchmarking to be completed in a straight forward and standardised way. Furthermore, caution should be taken in benchmarking a model using a single forcing data set. As part of the Land Surface, Snow and Soil Moisture Model Intercomparison Project (LS3MIP; van den Hurk et al., 2016) this configuration will be setup with GSWP3 forcing data, which in time will be made available to the community. A second dataset will allow sampling of model uncertainty arising from forcing data variation.

Surface albedo is simulated in the model as described in Section 2.2 Radiation. Globally the observed land surface albedo is generally higher in snow-covered regions and deserts as shown in the MODIS satellite data (Figure 6). As noted in Section 2.2.1 Diffuse Radiation, the simulated albedo in JULES-GL7.0 and 7.2 are exactly the same, despite having different canopy radiation options, as the differences only affect light availability for photosynthesis. Overall, we find the model is too bright with a globally positive bias (Table 4). However, Figure 7 shows that the bias is spatially variable with the largest biases (both positive and negative) found in the high latitudes and other snow-covered regions. In general, in this experimental setup we find the surface is too bright in regions of boreal forests and too dark across the far north in the tundra regions.

Evapotranspiration is benchmarked against two observational products: GLEAM (Miralles et al., 2011) and MODIS (Mu et al., 2013). There is uncertainty in the two datasets with large differences in the magnitude of evapotranspiration particularly over the tropical regions (Figure 8). Both GL7.0 and 7.2 have large positive biases over much of the world, and these are strongest over the tropics (up to 2mm per day; 9). However, the exact location of the largest biases differs between MODIS and GLEAM. GLEAM suggests a dipole pattern over central Africa while MODIS has a centralised positive bias implying there is a degree of observational uncertainty that needs to be accounted for. Overall, the biases are slightly reduced in GL7.2 (Table 4).

Although GL7 is mainly intended for studying the exchange of momentum, heat and water, the configuration also underpins the carbon-cycle configuration, and photosynthesis is strongly linked to evapotranspiration through the stomatal conductance model. It is therefore worth benchmarking the model's ability to simulate GPP. Here we compare simulated GPP against the Fluxnet-MTE product (Figure 10; Jung et al., 2010). Figure Figure 11 shows that GL7.0 and 7.2 correctly predict that GPP is highest in tropical forests and low in arid areas, but there is a substantial negative bias in most biomes with the exception of

tropical forests. GL7.2 is an improvement over GL7.0 with a global total GPP of 95.4 GtC compared with 91.1 GtC in GL7.0. However, this is substantially lower than the 119 GtC in the reference dataset.

5 Summary

JULES-GL7.0 is the standalone version of the land surface configuration underpinning the HadGEM3-GC3.1 climate model that is being run as part of the CMIP6 round of global climate modelling experiments. It is a comprehensive model simulating the exchange of heat, water and momentum developed as part of the coupled climate model and extracted here for use by the community.

It has been shown that both JULES-GL7.0 and JULES-GL7.2 can capture the large-scale features of surface albedo, evapotranspiration and GPP, however there are substantial biases that future updates to the configuration should attempt to reduce. There is also substantial uncertainty in observational evaluation datasets and the forcing for driving the model (Collier et al. 2018), which remains to be accounted for. Caution therefore needs to be taken to avoid overfitting the model to just a few datasets without a full appreciation of the uncertainties involved. In time, we plan to add additional forcing datasets to the standard configuration and the ability to benchmark against the full capability available in ILAMB.

This configuration and the ability to run the model is provided to the land surface modelling community to promote community engagement in the advancement of land surface science whether through application in their individual study, for use in model intercomparison studies such as LS3MIP (van den Hurk et al., 2016) or to promote community science developments progressing onto the main JULES trunk and into the major science configurations that underpin weather and climate forecasting in the UK.

Author Contributions

AW coordinated the preparation of the JULES version of the coupled GL7 suite and manuscript. JE led the initial development and testing of the GL7 configuration. AW, CDR, and KSD undertook the technical development to make the configuration available via JASMIN and the standardised suite control. AW, CDR, JE, NG, ABH, AH, MH and ER all prepared sections of the manuscript. All authors contributed to the preparation of the manuscript.

Acknowledgements

We thank Nicolas Viovy for providing the forcing data. This work was funded under the BEIS and DEFRA Met Office Hadley Centre Climate Programme (MOHCCP) for 2018 – 2021. AW and MCDR acknowledge the support of the EU Horizon 2020 CRECENDO project (grant agreement No 641816).

Data availability

The model configuration and associated forcing data are available via the indicated methods in the manuscript. JULES and associated configurations are freely available for non-commercial research use as set out in the JULES User Terms and Conditions (http://jules-lsm.github.io/access_req/JULES_Licence.pdf).

Code availability

This work is based on JULES version 5.3 with specific configurations included in the form of suites. For full information regarding accessing the code and configurations, please refer to Appendix A

References

Best, M. J.: Representing urban areas within operational numerical weather prediction models, Boundary-Layer Meteorol., 114(1), 91–109, doi:10.1007/s10546-004-4834-5, 2005.

Best, M. J., Pryor, M., Clark, D. B., Rooney, G. G., Essery, R. . L. H., Ménard, C. B., Edwards, J. M., Hendry, M. A., Porson, A., Gedney, N., Mercado, L. M., Sitch, S., Blyth, E., Boucher, O., Cox, P. M., Grimmond, C. S. B. and Harding, R. J.: The Joint UK Land Environment Simulator (JULES), model description – Part 1: Energy and water fluxes, Geosci. Model Dev., 4(3), 677–699, doi:10.5194/gmd-4-677-2011, 2011.

Betts, R. A., Boucher, O., Collins, M., Cox, P. M., Falloon, P. D., Gedney, N., Hemming, D. L., Huntingford, C., Jones, C. D., Sexton, D. M. H. and Webb, M. J.: Projected increase in continental runoff due to plant responses to increasing carbon dioxide, Nature, 448(7157), 1037–1041, doi:10.1038/nature06045, 2007.

Betts, R. A., Alfieri, L., Bradshaw, C., Caesar, J., Feyen, L., Friedlingstein, P., Gohar, L., Koutroulis, A., Lewis, K., Morfopoulos, C., Papadimitriou, L., Richardson, K. J., Tsanis, I. and Wyser, K.: Changes in climate extremes, fresh water availability and vulnerability to food insecurity projected at 1.5°C and 2°C global warming with a higher-resolution global climate model, Phil. Trans. R. Soc. A, 376(2119), 20160452, doi:10.1098/RSTA.2016.0452, 2018.

Clark, D. B., Mercado, L. M., Sitch, S., Jones, C. D., Gedney, N., Best, M. J., Pryor, M., Rooney, G. G., Essery, R. L. H., Blyth, E., Boucher, O., Harding, R. J., Huntingford, C. and Cox, P. M.: The Joint UK Land Environment Simulator (JULES), model description – Part 2: Carbon fluxes and vegetation dynamics, Geosci. Model Dev., 4(3), 701–722, doi:10.5194/gmd-4-701-2011, 2011.

Collatz, G., Ribas-Carbo, M. and Berry, J.: Coupled Photosynthesis-Stomatal Conductance Model for Leaves of C4 Plants, Funct. Plant Biol., 19(5), 519, doi:10.1071/PP9920519, 1992.

Collatz, G. J., Ball, J. T., Grivet, C. and Berry, J. A.: Physiological and environmental regulation of stomatal conductance, photosynthesis and transpiration: a model that includes a laminar boundary layer, Agric. For. Meteorol., 54(2–4), 107–136, doi:10.1016/0168-1923(91)90002-8, 1991.

Collier, N., Hoffman, F. M., Lawrence, D. M., Keppel-Aleks, G., Koven, C. D., Riley, W. J., Mu, M. and Randerson, J. T.: The International Land Model Benchmarking (ILAMB) System: Design, Theory, and Implementation, J. Adv. Model. Earth Syst., doi:10.1029/2018MS001354, 2018.

Collins, W. J., Bellouin, N., Doutriaux-Boucher, M., Gedney, N., Halloran, P., Hinton, T., Hughes, J., Jones, C. D., Joshi, M., Liddicoat, S., Martin, G., O'Connor, F., Rae, J., Senior, C., Sitch, S., Totterdell, I., Wiltshire, A. and Woodward, S.: Development and evaluation of an Earth-System model – HadGEM2, Geosci. Model Dev., 4(4), 1051–1075, doi:10.5194/gmd-4-1051-2011, 2011.

Cox, P. ., Huntingford, C. and Harding, R. .: A canopy conductance and photosynthesis model for use in a GCM land surface scheme, J. Hydrol., 212–213, 79–94, doi:10.1016/S0022-1694(98)00203-0, 1998.

Cox, P. M., R. A. Betts, C. B. Bunton, R. L. H. Essery, P. R. Rowntree, and J. Smith. "The impact of new land surface physics on the GCM simulation of climate and climate sensitivity." Climate Dynamics 15, no. 3 (1999): 183-203. 2

Dharssi, I., Vidale, P. L., Verhoef, A., Macpherson, B., Jones, C. and Best, M.: New soil physical properties implemented in the Unified Model at PS18, Meteorology Research and Development Technical Report 528, Met. Office, Exeter, UK, [online] Available from https://digital.nmla.metoffice.gov.uk/IO_01baed78-35d1-426d-aad0-88357bb493b2/ (Accessed 16 Sep 2019), 2009.Essery, R. L. H., Best, M. J., Betts, R. A., Cox, P. M., Taylor, C. M., Essery, R. L. H., Best, M. J., Betts, R. A., Cox, P. M. and Taylor, C. M.: Explicit Representation of Subgrid Heterogeneity in a GCM Land Surface Scheme, J. Hydrometeorol., 4(3), 530–543, doi:10.1175/1525-7541(2003)004<0530:EROSHI>2.0.CO;2, 2003.

Eyring, V., Bony, S., Meehl, G. A., Senior, C. A., Stevens, B., Stouffer, R. J. and Taylor, K. E.: Overview of the Coupled Model Intercomparison Project Phase 6 (CMIP6) experimental design and organization, Geosci. Model Dev., 9(5), 1937–1958, doi:10.5194/gmd-9-1937-2016, 2016.

Field, C. B., Jackson, R. B. and Mooney, H. A.: Stomatal responses to increased CO2: implications from the plant to the global scale, Plant, Cell Environ., 18(10), 1214–1225, doi:10.1111/j.1365-3040.1995.tb00630.x, 1995.

Gedney, N., Cox, P. M., Gedney, N. and Cox, P. M.: The Sensitivity of Global Climate Model Simulations to the Representation of Soil Moisture Heterogeneity, J. Hydrometeorol., 4(6), 1265–1275, doi:10.1175/1525-7541(2003)004<1265:TSOGCM>2.0.CO;2, 2003.

Van Genuchten, M.: A closed-form equation for predicting the hydraulic conductivity of unsaturated soils 1, Soil Sci. Am. J., 44, 892–898 [online] Available from: https://dl.sciencesocieties.org/publications/sssaj/abstracts/44/5/SS0440050892 (Accessed 4 December 2018), 1980.

Harper, A. B., Cox, P. M., Friedlingstein, P., Wiltshire, A. J., Jones, C. D., Sitch, S., Mercado, L. M., Groenendijk, M., Robertson, E., Kattge, J., Bönisch, G., Atkin, O. K., Bahn, M., Cornelissen, J., Niinemets, Ü., Onipchenko, V., Peñuelas, J., Poorter, L., Reich, P. B., Soudzilovskaia, N. A. and Van Bodegom, P.: Improved representation of plant functional types and physiology in the Joint UK Land Environment Simulator (JULES v4.2) using plant trait information, Geosci. Model Dev., 9(7), doi:10.5194/gmd-9-2415-2016, 2016.

van den Hurk, B., Kim, H., Krinner, G., Seneviratne, S. I., Derksen, C., Oki, T., Douville, H., Colin, J., Ducharne, A., Cheruy, F., Viovy, N., Puma, M. J., Wada, Y., Li, W., Jia, B., Alessandri, A., Lawrence, D. M., Weedon, G. P., Ellis, R., Hagemann, S., Mao, J., Flanner, M. G., Zampieri, M., Materia, S., Law, R. M. and Sheffield, J.: LS3MIP (v1.0) contribution to CMIP6: the Land Surface, Snow and Soil moisture Model Intercomparison Project – aims, setup and expected outcome, Geosci. Model Dev., 9(8), 2809–2832, doi:10.5194/gmd-9-2809-2016, 2016.

Jogireddy, V. ., Cox, P. M., Huntingford, C., Harding, R. J. and Mercado, L. M.: An improved description of canopy light interception for use in a GCM land-surface scheme: calibration and testing against carbon fluxes at a coniferous forest., 2003.

Jung, M., Reichstein, M., Ciais, P., Seneviratne, S. I., Sheffield, J., Goulden, M. L., Bonan, G., Cescatti, A., Chen, J., de Jeu, R., Dolman, A. J., Eugster, W., Gerten, D., Gianelle, D., Gobron, N., Heinke, J., Kimball, J., Law, B. E., Montagnani, L., Mu, Q., Mueller, B., Oleson, K., Papale, D., Richardson, A. D., Roupsard, O., Running, S., Tomelleri, E., Viovy, N., Weber, U., Williams, C., Wood, E., Zaehle, S. and Zhang, K.: Recent decline in the global land evapotranspiration trend due to limited moisture supply, Nature, 467(7318), 951–954, doi:10.1038/nature09396, 2010.

Jones, C.P.. Ancillary file generation for the UM. Unified Model Documentation Paper #73. Met Office Technical Documentation, 1998.

De Kauwe, M. G., Disney, M. I., Quaife, T., Lewis, P. and Williams, M.: An assessment of the MODIS collection 5 leaf area index product for a region of mixed coniferous forest, Remote Sens. Environ., 115(2), 767–780, doi:10.1016/J.RSE.2010.11.004, 2011.

Lehner, B., Verdin, K. and Jarvis, A.: HydroSHEDS technical documentation, version 1.0, HydroSHEDS Tech. Doc. (Version 1.0). World Wide Fund Nature, Washington, DC. URL http//gisdata.usgs.gov/webappcontent/HydroSHEDS/downloads/HydroSHEDS_TechDoc_v10.pdf [online] Available from: https://hydrosheds.cr.usgs.gov/HydroSHEDS_doc_v1_draft_dec7.doc (Accessed 4 December 2018), 2006.

Loveland, T. R. and Belward, A. S.: The IGBP-DIS global 1km land cover data set, DISCover: First results, Int. J. Remote Sens., 18(15), 3289–3295, doi:10.1080/014311697217099, 1997.

Manners, J., Edwards, J. M., Hill, P. and Thelen, J.: SOCRATES Technical Guide Suite Of Community RAdiative Transfer codes based on Edwards and Slingo, Tech Reports Met Off. UK. [online] Available from: http://homepages.see.leeds.ac.uk/~lecsjed/winscpuse/socrates_techguide.pdf (Accessed 9 May 2019), 2017.

Marthews, T. R., Dadson, S. J., Lehner, B., Abele, S. and Gedney, N.: High-resolution global topographic index values for use in large-scale hydrological modelling, Hydrol. Earth Syst. Sci., 19(1), 91–104, doi:10.5194/hess-19-91-2015, 2015.

Martin, G. M., Bellouin, N., Collins, W. J., Culverwell, I. D., Halloran, P. R., Hardiman, S. C., Hinton, T. J., Jones, C. D., McDonald, R. E., McLaren, A. J., O'Connor, F. M., Roberts, M. J., Rodriguez, J. M., Woodward, S., Best, M. J., Brooks, M.

E., Brown, A. R., Butchart, N., Dearden, C., Derbyshire, S. H., Dharssi, I., Doutriaux-Boucher, M., Edwards, J. M., Falloon, P. D., Gedney, N., Gray, L. J., Hewitt, H. T., Hobson, M., Huddleston, M. R., Hughes, J., Ineson, S., Ingram, W. J., James, P. M., Johns, T. C., Johnson, C. E., Jones, A., Jones, C. P., Joshi, M. M., Keen, A. B., Liddicoat, S., Lock, A. P., Maidens, A. V., Manners, J. C., Milton, S. F., Rae, J. G. L., Ridley, J. K., Sellar, A., Senior, C. A., Totterdell, I. J., Verhoef, A., Vidale, P. L.

5   and Wiltshire, A.: The HadGEM2 family of Met Office Unified Model climate configurations, Geosci. Model Dev., 4(3), doi:10.5194/gmd-4-723-2011, 2011.

Mercado, L. M., Huntingford, C., Gash, J. H. C., Cox, P. M. and Jogireddy, V.: Improving the representation of radiation interception and photosynthesis for climate model applications, Tellus B Chem. Phys. Meteorol., 59(3), 553–565, doi:10.1111/j.1600-0889.2007.00256.x, 2007.

10   Miralles, D., Holmes, T., Jeu, R. De and Gash, J.: Global land-surface evaporation estimated from satellite-based observations, [online] Available from: http://dare.ubvu.vu.nl/bitstream/handle/1871/39825/277927.pdf?sequence=1 (Accessed 11 April 2019), 2011.

Mu, Q., Zhao, M. and Running, S.: MODIS global terrestrial evapotranspiration (ET) product (NASA MOD16A2/A3) collection 5. NASA Headquarters, [online] Available from: https://scholarworks.umt.edu/ntsg_pubs/268/ (Accessed 11 April

15   2019), 2013.

Osborne, T., Gornall, J., Hooker, J., Williams, K., Wiltshire, A., Betts, R. and Wheeler, T.: JULES-crop: A parametrisation of crops in the Joint UK Land Environment Simulator, Geosci. Model Dev., 8(4), doi:10.5194/gmd-8-1139-2015, 2015.

Le Quéré, C., Moriarty, R., Andrew, R. M., Canadell, J. G., Sitch, S., Korsbakken, J. I., Friedlingstein, P., Peters, G. P., Andres, R. J., Boden, T. A., Houghton, R. A., House, J. I., Keeling, R. F., Tans, P., Arneth, A., Bakker, D. C. E., Barbero, L., Bopp,

20   L., Chang, J., Chevallier, F., Chini, L. P., Ciais, P., Fader, M., Feely, R. A., Gkritzalis, T., Harris, I., Hauck, J., Ilyina, T., Jain, A. K., Kato, E., Kitidis, V., Klein Goldewijk, K., Koven, C., Landschützer, P., Lauvset, S. K., Lefèvre, N., Lenton, A., Lima, I. D., Metzl, N., Millero, F., Munro, D. R., Murata, A., S. Nabel, J. E. M., Nakaoka, S., Nojiri, Y., O'Brien, K., Olsen, A., Ono, T., Pérez, F. F., Pfeil, B., Pierrot, D., Poulter, B., Rehder, G., Rödenbeck, C., Saito, S., Schuster, U., Schwinger, J., Séférian, R., Steinhoff, T., Stocker, B. D., Sutton, A. J., Takahashi, T., Tilbrook, B., Van Der Laan-Luijkx, I. T., Van Der

25   Werf, G. R., Van Heuven, S., Vandemark, D., Viovy, N., Wiltshire, A., Zaehle, S. and Zeng, N.: Global Carbon Budget 2015, Earth Syst. Sci. Data, 7(2), doi:10.5194/essd-7-349-2015, 2015.

Le Quéré, C., Andrew, R. M., Friedlingstein, P., Sitch, S., Pongratz, J., Manning, A. C., Ivar Korsbakken, J., Peters, G. P., Canadell, J. G., Jackson, R. B., Boden, T. A., Tans, P. P., Andrews, O. D., Arora, V. K., Bakker, D. C. E., Barbero, L., Becker, M., Betts, R. A., Bopp, L., Chevallier, F., Chini, L. P., Ciais, P., Cosca, C. E., Cross, J., Currie, K., Gasser, T., Harris, I.,

30   Hauck, J., Haverd, V., Houghton, R. A., Hunt, C. W., Hurtt, G., Ilyina, T., Jain, A. K., Kato, E., Kautz, M., Keeling, R. F., Klein Goldewijk, K., Körtzinger, A., Landschützer, P., Lefèvre, N., Lenton, A., Lienert, S., Lima, I., Lombardozzi, D., Metzl, N., Millero, F., Monteiro, P. M. S., Munro, D. R., Nabel, J. E. M. S., Nakaoka, S.-I., Nojiri, Y., Antonio Padin, X., Peregon, A., Pfeil, B., Pierrot, D., Poulter, B., Rehder, G., Reimer, J., Rödenbeck, C., Schwinger, J., Séférian, R., Skjelvan, I., Stocker, B. D., Tian, H., Tilbrook, B., Tubiello, F. N., Laan-Luijkx, I. T. V., Werf, G. R. V., Van Heuven, S., Viovy, N., Vuichard, N.,

35   Walker, A. P., Watson, A. J., Wiltshire, A. J., Zaehle, S. and Zhu, D.: Global Carbon Budget 2017, Earth Syst. Sci. Data, 10(1), doi:10.5194/essd-10-405-2018, 2018.

Sellars, P. J.: Canopy reflectance, photosynthesis and transpiration, Int. J. Remote Sens., 6(8), 1335–1372, doi:10.1080/01431168508948283, 1985.

Sellers, P. J., Bounoua, L., Collatz, G. J., Randall, D. A., Dazlich, D. A., Los, S. O., Berry, J. A., Fung, I., Tucker, C. J., Field,

40   C. B. and Jensen, T. G.: Comparison of Radiative and Physiological Effects of Doubled Atmospheric CO2 on Climate, Science (80-.)., 271(5254), 1402–1406, doi:10.1126/science.271.5254.1402, 1996.

Shannon, S., Smith, R., Wiltshire, A., Payne, T., Huss, M., Betts, R., Caesar, J., Koutroulis, A., Jones, D. and Harrison, S.: Global glacier volume projections under high-end climate change scenarios, Cryosph. Discuss., 1–36, doi:10.5194/tc-2018-

35, 2018.

Taillandier, A.-S., Domine, F., Simpson, W. R., Sturm, M. and Douglas, T. A.: Rate of decrease of the specific surface area of dry snow: Isothermal and temperature gradient conditions, J. Geophys. Res., 112(F3), F03003, doi:10.1029/2006JF000514, 2007.

5 Walters, D., Baran, A., Boutle, I., Brooks, M., Earnshaw, P., Edwards, J., Furtado, K., Hill, P., Lock, A., Manners, J., Morcrette, C., Mulcahy, J., Sanchez, C., Smith, C., Stratton, R., Tennant, W., Tomassini, L., Van Weverberg, K., Vosper, S., Willett, M., Browse, J., Bushell, A., Dalvi, M., Essery, R., Gedney, N., Hardiman, S., Johnson, B., Johnson, C., Jones, A., Mann, G., Milton, S., Rumbold, H., Sellar, A., Ujiie, M., Whitall, M., Williams, K. and Zerroukat, M.: The Met Office Unified Model Global Atmosphere 7.0/7.1 and JULES Global Land 7.0 configurations, Geosci. Model Dev. Discuss., 1–78, doi:10.5194/gmd-
10 2017-291, 2017.

Walters, D. N., Best, M. J., Bushell, A. C., Copsey, D., Edwards, J. M., Falloon, P. D., Harris, C. M., Lock, A. P., Manners, J. C., Morcrette, C. J., Roberts, M. J., Stratton, R. A., Webster, S., Wilkinson, J. M., Willett, M. R., Boutle, I. A., Earnshaw, P. D., Hill, P. G., MacLachlan, C., Martin, G. M., Moufouma-Okia, W., Palmer, M. D., Petch, J. C., Rooney, G. G., Scaife, A. A. and Williams, K. D.: The Met Office Unified Model Global Atmosphere 3.0/3.1 and JULES Global Land 3.0/3.1
15 configurations, Geosci. Model Dev., 4(4), 919–941, doi:10.5194/gmd-4-919-2011, 2011.

Williams, K. D., Copsey, D., Blockley, E. W., Bodas-Salcedo, A., Calvert, D., Comer, R., Davis, P., Graham, T., Hewitt, H. T., Hill, R., Hyder, P., Ineson, S., Johns, T. C., Keen, A. B., Lee, R. W., Megann, A., Milton, S. F., Rae, J. G. L., Roberts, M. J., Scaife, A. A., Schiemann, R., Storkey, D., Thorpe, L., Watterson, I. G., Walters, D. N., West, A., Wood, R. A., Woollings, T. and Xavier, P. K.: The Met Office Global Coupled Model 3.0 and 3.1 (GC3.0 and GC3.1) Configurations, J. Adv. Model.
20 Earth Syst., 10(2), 357–380, doi:10.1002/2017MS001115, 2018.

Yang, W., Tan, B., Huang, D., Rautiainen, M., Shabanov, N. V., Wang, Y., Privette, J. L., Huemmrich, K. F., Fensholt, R., Sandholt, I., Weiss, M., Ahl, D. E., Gower, S. T., Nemani, R. R., Knyazikhin, Y. and Myneni, R. B.: MODIS leaf area index products: From validation to algorithm improvement, IEEE Trans. Geosci. Remote Sens., 44(7), 1885–1896, doi:10.1109/TGRS.2006.871215, 2006.

Tables

Table 1: Parameters in JULES-GL7 that vary with non-vegetated surface types (note these can be found in nvegparm).

	Urban	Lake	Bare Soil	Ice
albsnf *Snow-free albedo*	0.18	0.12	-1 (indicates read *from* ancillary)	0.75
catch *Water capacity (kg m^{-2})*i	0.5	0	0	0
ch *Heat capacity of this surface type (J K^{-1}m^{-2}).*	280000	21100000	0	0
emis *Surface emissivity*	0.97	0.985	0.9	0.99
gs *Surface conductance (m s^{-1}).*	0	0	0.01	1000000
infil *Infiltration enhancement factor*	0.1	0	0.5	0
vf *Switch indictaing whether the canopy is conductivity coupled (0) to the sub-surface or radiatively (1).*	1	1	0	0
z0 *Roughness length for momentum (m)*	1	0.0001	0.001	0.0005
z0hm *Ratio of the roughness length for heat to the roughness length for momentum.*	1E-07	0.25	0.02	0.2

5 **Table 2: Parameters in JULES-GL7 that vary by PFT (note these can be found in pftparm and snow namelists).**

	Broadleaf Tree	Needleleaf Tree	C3 Grass	C4 Grass	Shrub
a_wl *Allometric coefficient relating the target woody biomass to the leaf area index*	0.65	0.65	0.005	0.005	0.1
a_ws *Woody biomass as a multiple of live stem biomass.*	10	10	1	1	10
albsnc_max *Snow-covered albedo for large leaf area index.*	0.25	0.25	0.6	0.6	0.4

albsnc_min Snow-covered albedo for zero leaf area index.	0.3	0.3	0.8	0.8	0.8
alnir Leaf reflection coefficient for NIR	0.45	0.35	0.58	0.58	0.58
alpar Leaf reflection coefficient for PAR (photosynthetically active radiation)	0.1	0.07	0.1	0.1	0.1
alpha Quantum efficiency (mol CO_2 per mol PAR photons).	0.08	0.08	0.08	0.04	0.08
b_wl Allometric exponent relating the target woody biomass to the leaf area index	1.667	1.667	1.667	1.667	1.667
c3 c3/c4 photosynthetic pathway switch	1	1	1	0	1
can_struct_a Canopy Structure factor	1	1	1	1	1
catch0 This is the minimum amount of water that can be held on the canopy (kg m^{-2})	0.5	0.5	0.5	0.5	0.5
dcatch_dlai Rate of change of canopy capacity with LAI (kg m^{-2}).	0.05	0.05	0.05	0.05	0.05
dqcrit Critical humidity deficit (kg H_2O per kg air).	0.09	0.06	0.1	0.075	0.1
dz0v_dh Rate of change of vegetation roughness length for momentum with height.	0.05	0.05	0.1	0.1	0.1
emis_pft Surface emissivity	0.98	0.99	0.98	0.98	0.98
eta_sl Live stemwood coefficient (kg Cm^{-1}/(m2 leaf))	0.01	0.01	0.01	0.01	0.01
f0 Ratio of internal to atmospheric CO2 concentration at 0. Humidity deficit (CI / CA for DQ = 0)	0.875	0.875	0.9	0.8	0.9
fd Scale factor for dark respiration.	0.015	0.015	0.015	0.025	0.015
fsmc_mod	0	0	0	0	0

Switch for method of weighting the contribution that different soil layers make to the soil moisture availability factor fsmc.					
glmin *Minimum leaf conductance for H₂O (m s⁻¹).*	0.000001	0.000001	0.000001	0.000001	0.000001
infil_f *Infiltration enhancement factor*	4	4	2	2	2
kext *Light extinction coefficient*	0.5	0.5	0.5	0.5	0.5
knl *Parameter for decay of nitrogen through the canopy, as a function of LAI*	0.2	0.2	0.2	0.2	0.2
kpar *PAR extinction coefficient*	0.5	0.5	0.5	0.5	0.5
lai_alb_lim *Minimum LAI permitted in calculation of the albedo in snow-free conditions.*	0.005	0.005	0.005	0.005	0.005
nl0 *Top leaf nitrogen concentration (kg N/kg C).*	0.04	0.03	0.06	0.03	0.03
neff *Scale factor relating Vcmax with leaf nitrogen concentration*	0.0008	0.0008	0.0008	0.0004	0.0008
nr_nl *Ratio of root nitrogen concentration to leaf nitrogen concentration.*	1	1	1	1	1
ns_nl *Ratio of stem nitrogen concentration to leaf nitrogen concentration.*	0.1	0.1	1	1	0.1
omega *Leaf scattering coefficient for PAR.*	0.15	0.15	0.15	0.17	0.15
omnir *Leaf scattering coefficient for NIR.*	0.7	0.45	0.83	0.83	0.83
orient	0	0	0	0	0
q10_leaf *Q10 factor for plant respiration.*	2	2	2	2	2
r_grow *Growth respiration fraction.*	0.25	0.25	0.25	0.25	0.25
rootd_ft	3	1	0.5	0.5	0.5

Parameter determining the root depth (m).					
sigl *Specific density of leaf carbon (kg C m^{-2}leaf).*	0.0375	0.1	0.025	0.05	0.05
Tlow *Lower temperature for photosynthesis (deg C).*	0	-5	0	13	0
Tupp *Upper temperature for photosynthesis (deg C).*	36	31	36	45	36
z0hm_pft *Ratio of the roughness length for heat to the roughness length for momentum.*	1.65	1.65	0.1	0.1	0.1
Snow Parameters					
can_clump *Clumping factor for snow in the canopy*	1	4	1	1	1
cansnowpft *Canopy snow model switch*	.false.	.true.	.false.	.false.	.false
lai_alb_lim_sn *Lower limit on permitted LAI in albedo with snow*	1	1	0.1	0.1	0.1
n_lai_exposed *Shape parameter for exposed canopy with embedded snow*	1	1	3	3	2
unload_rate_cnst *Constant canopy snow unloading rate (kg m^{-2} s^{-1})*	0	0	0	0	0
unload_rate_u *Wind dependent canopy snow unloading rate (kg m^{-2}s^{-1}snow per ms^{-1} wind)*	0	2.31E-06	0	0	0

Table 3: Ancillary information as required in the JULES-GL7.0/7.2 Configurations. Required ancillary files cover parameter values that are either spatially or temporarily explicit necessary to define the science configuration. Additional ancillaries covering grid setup and forcing are used in the experimental setup.

File	Fields and Description
Science Configuration	
Landcover Fractions	frac: Spatial fractional cover of each landcover tile
Vegetation Function	canht: Canopy height for vegetation tiles
	lai: Monthly Leaf Area Index Climatology for vegetation tiles
Soil properties	albsoil. Average waveband spatial field
	b: van Genuchten soil hydraulic parameter (1/(n-1))
	hcap: Dry heat capacity
	satcon: Saturated hydraulic conductivity
	sathh: van Genuchten soil hydraulic 1/alpha parameter
	smcrit: volumetric soil moisture critical point
	smsat:saturated volumentric soil mositire
	smwilt: volumetric soil moisture wilting point
Hydrology	timean: spatial mean in topographic index
	tisig: spatial standard deviation in topographic index
Experimental Setup	
Land Fraction	Land_frac: fraction of a gridbox that is land

Table 4: Tabulated measures of model performance against benchmarks. Global Means and Totals are calculated on the native grid of the observational and model grids accounting for fractional land coverage in the totals and weighting for irregular grid box sizes. Biases and RMSEs are calculated by regridding the observational data to the coarser model grid and calculating metrics where the observational and model data intersect.

	Global Means/Totals	Bias	RMSE
MODIS Albedo (Dimensionless)			
Benchmark	0.20		
GL7.0	0.25	0.039	0.074
GLEAM Evapotranspiration (mm day^{-1})			
Benchmark	1.29		
GL7.0	1.72	0.35	0.65
GL7.2	1.70	0.33	0.62
MODIS Evapotranspiration (mm day^{-1})			
Benchmark	1.57		
GL7.0	1.73	0.38	0.63
GL7.2	1.71	0.36	0.62
Fluxnet-MTE Gross primary Productivity (gC m^{-2} day^{-1})			
Benchmark	119 GtC		
GL7.0	91.1 GtC	-0.6	1.06
GL7.2	95.4 GtC	-0.5	0.99
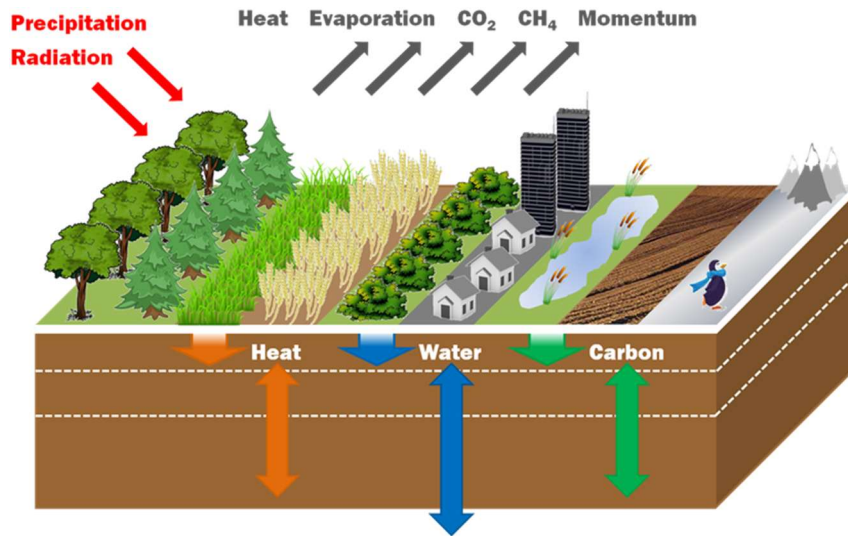
Figures

5   **Figure 1. JULES schematic of the fluxes of stores of heat, water, carbon and momentum and the surface tiling representation of subgrid heterogeneity.**
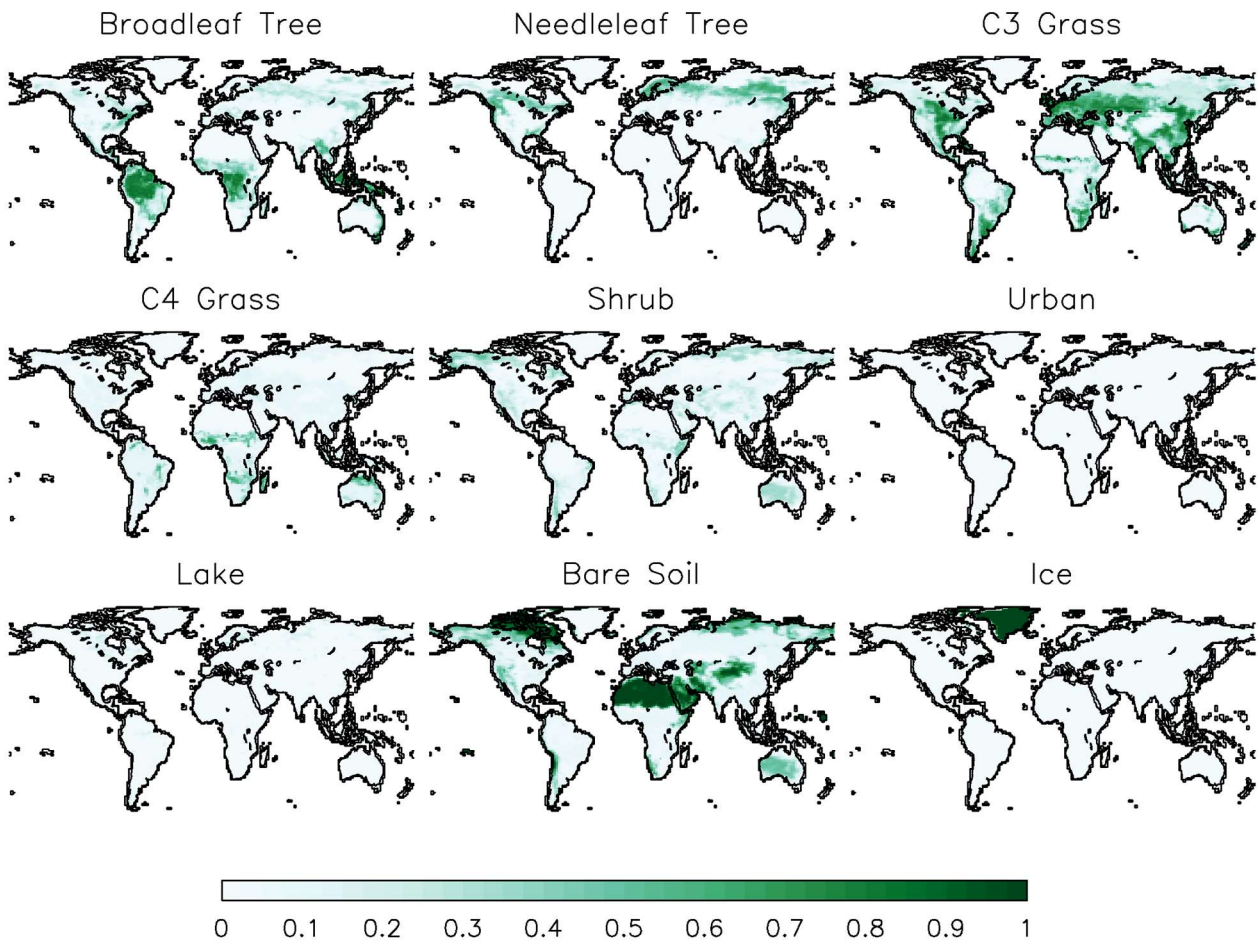
Figure 2. Surface Tile fractions as used in JULES-GL7 derived from the IGBP landcover dataset (IGBP: Global Soil Data Task,
10   **2000)**
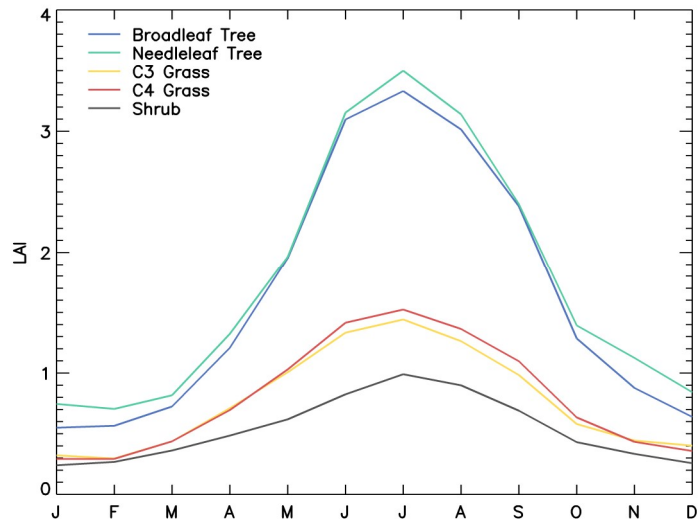
Figure 3. Seasonal Leaf Area Index (LAI) for the 5 vegetation surface types area-averaged over 30-60°N.
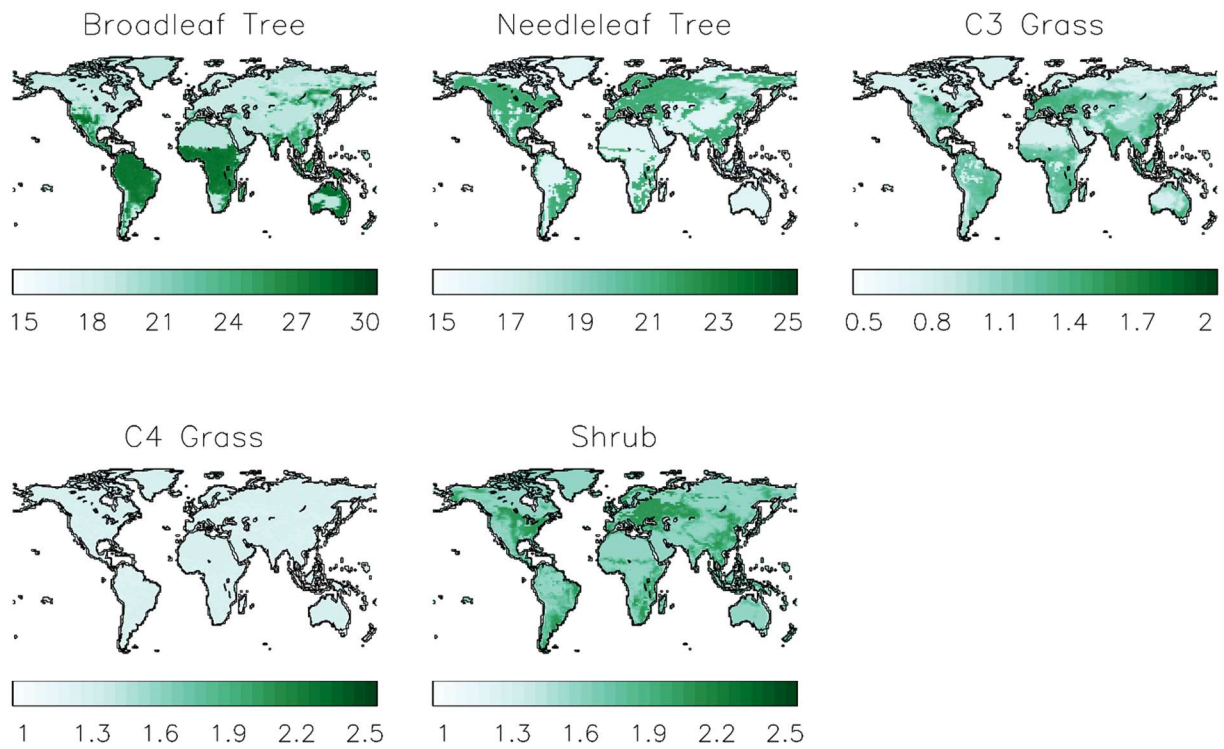
Figure 4. Canopy Height (m) per Plant Functional Type (PFT) as used in JULES-GL7 derived from the IGBP landcover dataset (IGBP: Global Soil Data Task, 2000).
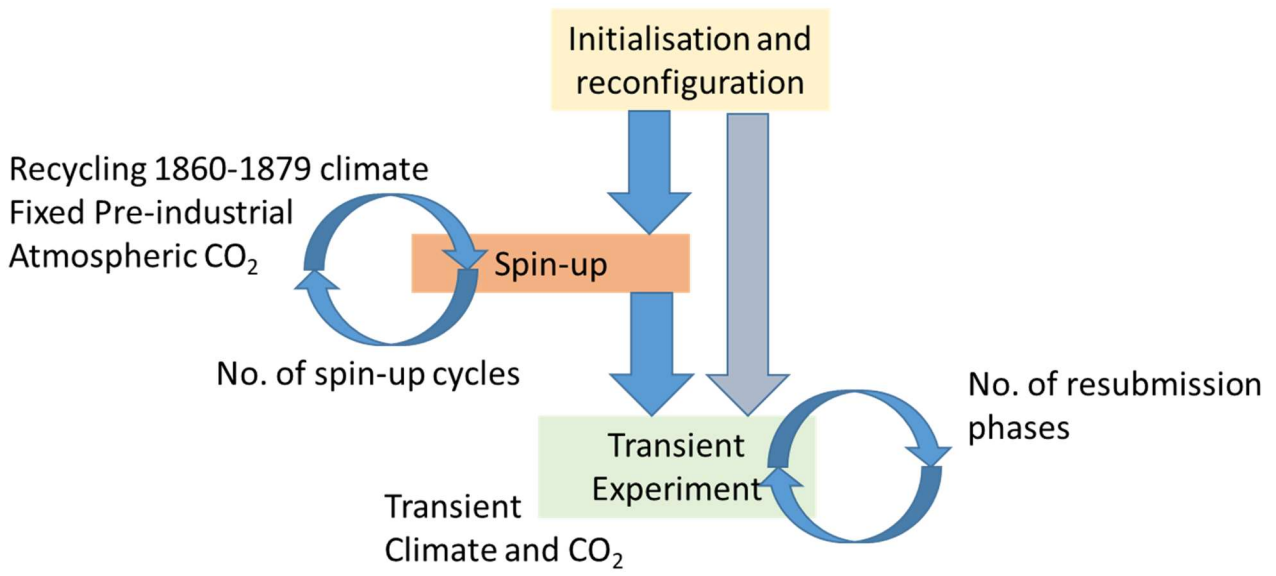
Figure 5: Suite control used to initialise, spinup and perform a full transient experiment with JULES-GL7.
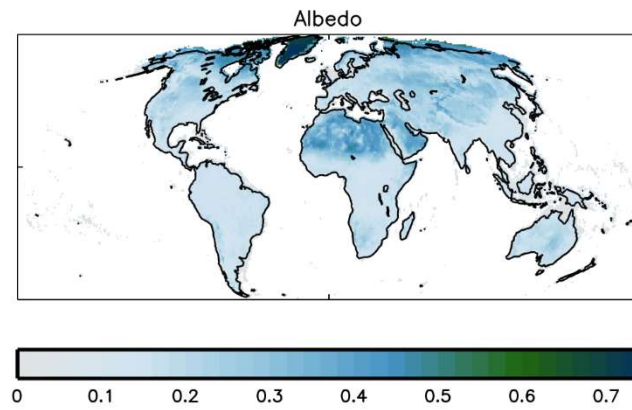
Figure 6: Surface albedo 2000-2005 benchmark derived from MODIS (De Kauwe et al., 2011) as generated by ILAMB (Collier et al., 2018).
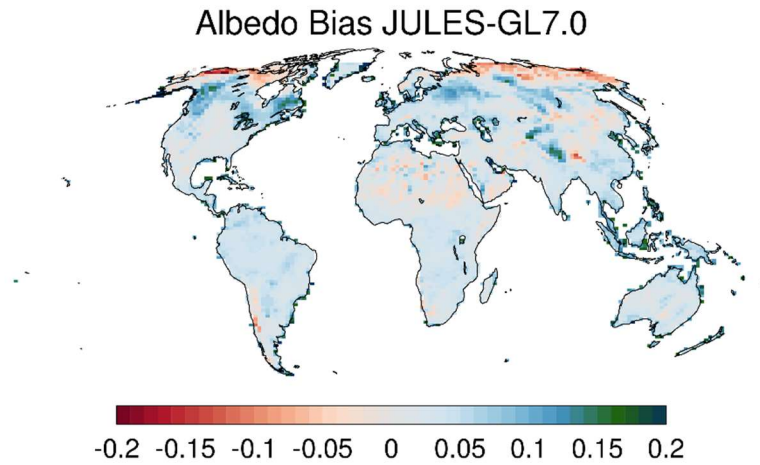
Figure 7: Albedo bias simulated by GL7.0 relative to the MODIS benchmark. Means over 2000-2005 are shown. Biases are calculated as the difference between the model and observations.
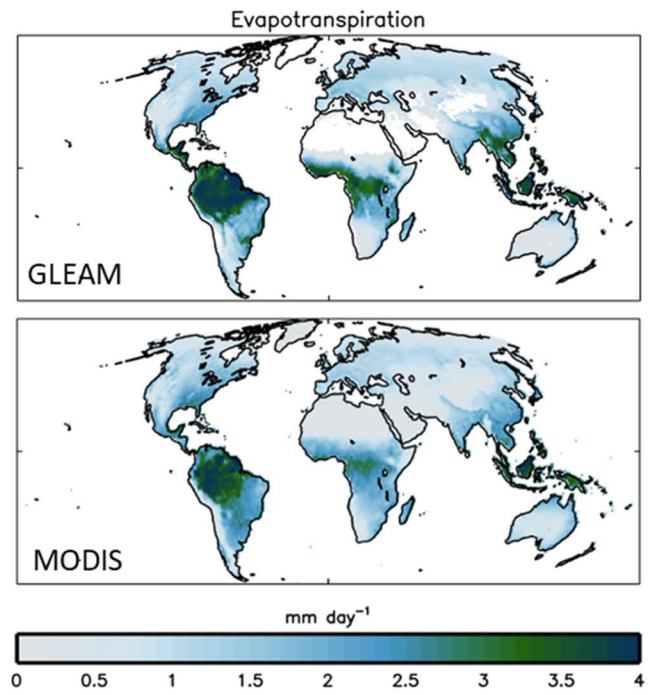
Figure 8: Surface evapotranspiration benchmarks derived from GLEAM (Miralles et al., 2011) and MODIS (Mu et al., 2013) as generated by ILAMB (Collier et al., 2018) covering 1980-2011 and 2000-2013 respectively.
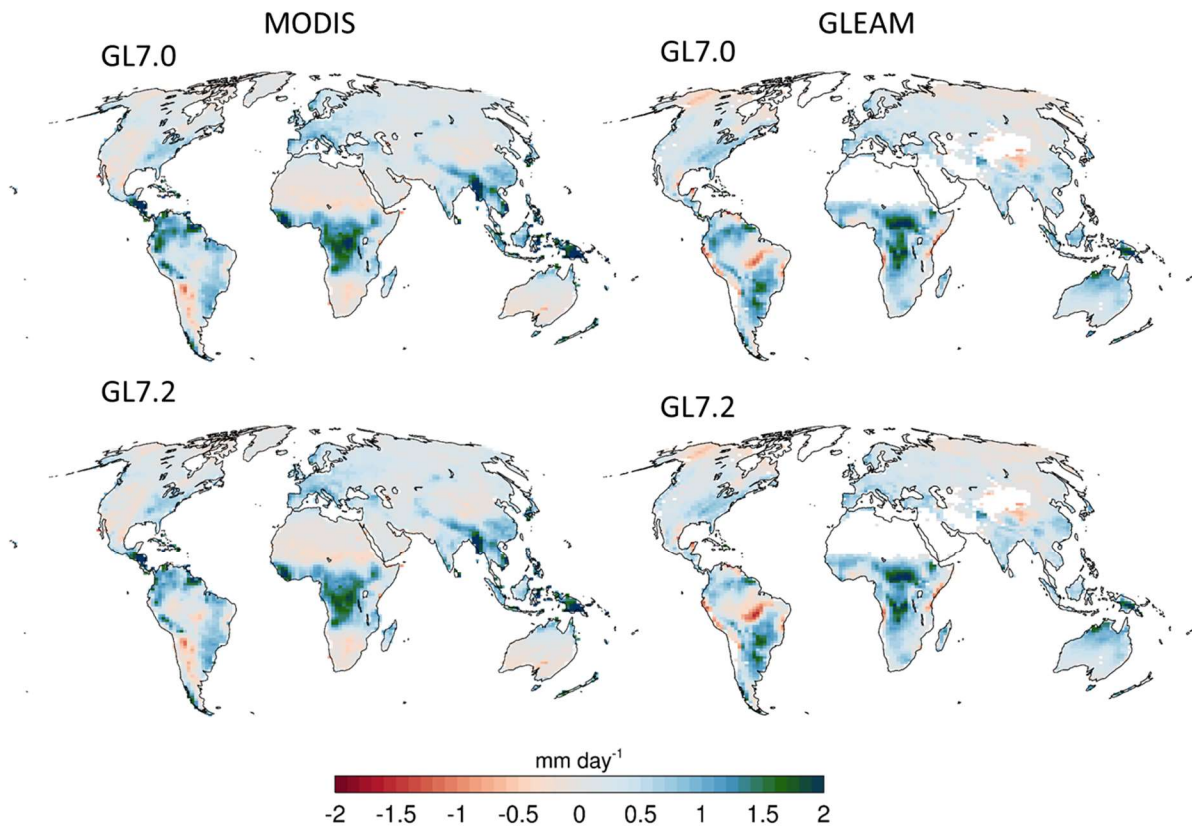
Figure 9: Evapotranspiration biases simulated by GL7.0 (top row) and GL7.2 (bottom row) for MODIS (left column) and GLEAM (right column) benchmarks. MODIS means are 2000-2013 and GLEAM 1980-2011. Biases are calculated as the difference between the model and observations.
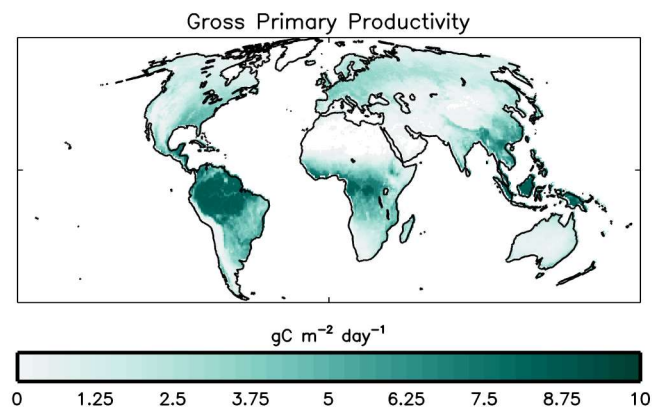
Figure 10: Global Primary Productivity (GPP) (1982-2008) benchmark derived from Fluxnet- MTE (Jung et al., 2010) as generated by ILAMB (Collier et al., 2018).
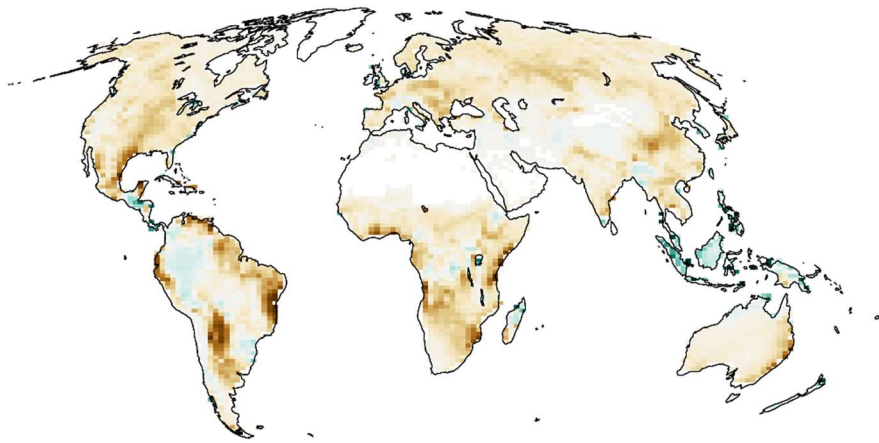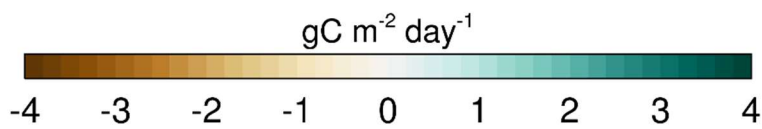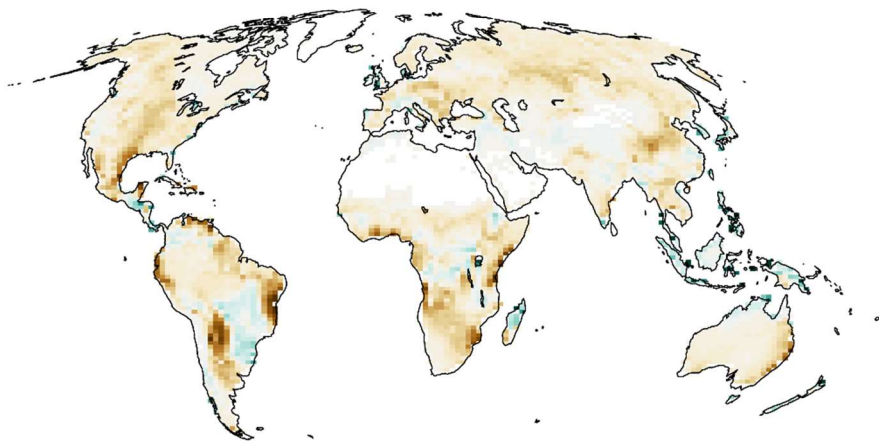
Figure 11: Global Primary Productivity (GPP) biases simulated by GL7.0 (top row) and GL7.2 (bottom row) against the Fluxnet-MTE dataset. Means are 1982-2008. Biases are calculated as the difference between the model and observations.

Appendix A: Running JULES-GL7

This section describes how to access and run the JULES-GL7.0 and JULES-GL7.2 suites provided at JULES version 5.3. It is recommended that the latest version is used available from (https://code.metoffice.gov.uk/trac/jules/wiki/JulesConfigurations, login required) to benefit. to benefit from bug fixes, ease of testing and implementing developments, which can only take place

5   at the head of the JULES code trunk.

A.1 Compute Platform Setup

The JULES-GL7.0 and JULES-GL7.2 configurations are available as Rose suites at https://code.metoffice.gov.uk/trac/roses-u/browser/b/b/3/1/6/trunk and https://code.metoffice.gov.uk/trac/roses-u/browser/b/b/5/4/3/trunk respectively. Note, access will be required to the Met Office Science Repository Service (https://code.metoffice.gov.uk/trac/home) and is available to

10   those who have signed the JULES user agreement. JULES is freely available for non-commercial research use as set out in the JULES User Terms and Conditions (http://jules-lsm.github.io/access_req/JULES_Licence.pdf). The easiest way to access the repository is by completing the online form here (http://jules-lsm.github.io/access_req/JULES_access.html).

The suite is configured to run on both the Met Office CRAY XC40 or the JASMIN (http://www.jasmin.ac.uk/) platform

15   provided by the Science and Technology Facilities Council UK. For non-Met Office collaborators JASMIN is the most suitable platform for running JULES simulations. JASMIN access is available for all UK based researchers who consider themselves part of the NERC (https://nerc.ukri.org/) community. JASMIN is also available for non-UK based researchers who are interested in JULES. Once you have access to JASMIN you will need to request access to the JULES group workspace (/group_workspaces/jasmin2/jules), which can be requested here

20   https://accounts.jasmin.ac.uk/services/group_workspaces/jules/. Met Office CRAY XC40 users will need access to the xcel00 and/or xcef00 machines.

Installing the suite requires access to the Met Office suite and code management tools available on both JASMIN and the Met Office Linux estate. To access the tools please follow the guidelines in Appendix A.5. Once you have access to the necessary

25   compute platforms, repository and tools you are ready to start your run.

The suite is designed for ease of use, to enable the maximum number of users to access it. The suite is configured to extract the code from the repository, build on the appropriate platform sourcing appropriate libraries and then run using the appropriate forcing and ancillaries. Most users should be able to set a standard run going in just a few steps.

30   **A.2 Setting up the model configuration**

The standard JULES-GL7.0 (*JULES-GL7.2*) suite, u-bb316, (*u-bb543*) has been configured to minimise the steps necessary to be able to run the standard configuration, however a few important steps and checks remain. It is assumed that a JASMIN user has logged into the jasmin-cylc node and a Met Office user is accessing the CRAY via a Linux desktop.

    1. Create a new suite:

35   *rosie copy u-bb316*

          This will create a new suite of your own in which changes can be made and tracked using the Met Office Science Repository Service. Remember to commit any changes back to the repository with '*fcm commit.*' *Rosie copy u-bb316* results in a new suite with a similar id in alphanumeric order e.g. *u-ab123*. You should replace '*u-ab123*' with your suite id in the following commands.

40

2. The *rosie copy* command will create a local copy of the new suite in the *~/roses* directory. You can change directory to this suite.

3. Once the suite is installed you can use the Rose GUI editor to check the suite setup. There are a number of platform specific aspects to be checked. To open the GUI:

    rose edit -C ~/roses/u-ab123/

    a. Build options > JULES_FCM – This variable points to the location of the code to be compiled. In the standard case this should point to the trunk, however this could equally point to a branch to test a new development. An important point to note is that the CRAY uses an internal 'mirror' copy of the repository held in the cloud. This avoids downtime when the repository is unavailable. This is indicated by an '*m*' in the repository shortcuts. This should be *fcm:jules.xm* and *fcm:jules.x* on the CRAY and JASMIN respectively. This is handled in the background by the Cylc control system, however failure to set this correctly will result in a build failure.

    b. Platform specific > Build and run mode – This radar button is used to setup the platform specific build and installation. This should be '*Met Office-cray-xc40*' and '*Jasmin-Lotus*' on the CRAY and JASMIN platforms respectively.

    c. Runtime Configuration > MPI_NUM_TASKS – Up to 16 MPI tasks are available on JASMIN. More are available on the CRAY for faster run times. 16 MPI tasks is a recommended setup. However, 18 MPI (with 2 OMP) makes a fuller user of a single broadwell node on the CRAY.

    d. Runtime Configuration > OMP_NUM_TASKS – More recently releases of JULES support more OpenMP threads. A suitable number of tasks is 2.

    The suite is now installed and ready to run. On the CRAY the submission can be made from the local machine. On JASMIN use the Cylc workflow machine *jasmin-cylc*. The suite can be submitted to the scheduler.

    rose suite-run -C ~/roses/u-ab123/

4. Assuming the suite submits correctly, the next step is to monitor progress. Met Office and JASMIN users will automatically see the *suite control GUI*. However, the suite can be monitored by one of the two following options:

    cylc scan –c   Will show the state of running suites
    tail -f ~/cylc-run/u-ab123/log/suite/log   Will print to screen the current status of u-ab123

5. The output from the suite is automatically written to a directory:
    a. *$DATADIR/jules_output/u-ab123* on the CRAY
    b. */work/scratch/$USER/u-ab123* on JASMIN.

    Note the scratch workspace on JASMIN is not for permanent storage of model output.

A.3 Making changes to model configuration

The purpose of making a standard science configuration and experimental setup available is not so users can reproduce the same results, but to encourage further development and testing, whether that involves new and novel diagnostics and evaluation or new processes and ancillary information. This should be done relative to the 'benchmark' standard configuration and experimental setup. To modify the configurations users should copy the standard suite as above and switch the code base to point to the user's branch and revision number. Any new parameters and switches can then be added to the app configuration

file – this can be done through the GUI or by editing the configuration file directly (*~/roses/u-ab123/app/rose-suite.conf*). Note the model code needs to be consistent with the setup in the app. Any modifications to the suite should be committed and documented on a JULES ticket similar to the one documenting the JULES-GL7 release (https://code.metoffice.gov.uk/trac/jules/ticket/837).

5   Model developers should use the suite and information presented here in combination with the JULES technical documentation found in Best et al., (2011) and Clark et al., (2011).

A.4 Inter-version compatibility

The JULES-GL7 model configurations are independent of the code release as it is a requirement of any modification to the
10   JULES code base that the major configurations are scientifically reproducible between code versions. This is not exactly the same as reproducible to the bit level as some changes are permitted, for instance changing the order of a do loop can have benefits for runtime, but lead to changes are the bit level. From a user perspective the differences between model releases should be pragmatically indistinguishable. It is intended that the JULES-GL7 configurations will be made available at each model release and the latest release is preferable if undertaking configuration development. Users of the configuration may
15   find benefits in the latest version through technical improvements to suite control tools including user interfaces and code optimisation reducing run time. It is therefore preferable to use the latest available configuration. At some point when a configuration is deemed superseded the guarantee of backwards compatibility will be dropped and code modules may be removed from the code base and no longer supported.

20   ## A.5: Setting up the JASMIN work environment.

The following assumes you have access to JASMIN as outlined in Section 5. This section outlines the necessary steps to setup the necessary work environment.

On `jasmin-cylc`, edit your `~/.bash_profile` file:

```
# Get the aliases and functions

if [ -f ~/.bashrc ]; then
        . ~/.bashrc
fi

# User specific environment and startup programs

export PATH=$PATH:$HOME/bin
HOST=$(hostname)

if [[ $HOST = "jasmin-sci2.ceda.ac.uk" || $HOST = "jasmin-cylc.ceda.ac.uk" || $HOST = "jasm
in-sci1.ceda.ac.uk" ]]; then
  # Rose/cylc on jasmin-sci & Lotus nodes
  export PATH=$PATH:/apps/contrib/metomi/bin
fi
```

On `jasmin-cylc` edit your `~/.bashrc` file at the top:

```
# Provide access to FCM, Rose and Cylc
PATH=$PATH:/apps/contrib/metomi/bin

# Ensure .bashrc is sourced in login shells
```

```
# (only add this if it is not already done in your .bash_profile)
[[ -f ~/.bashrc ]] && . ~/.bashrc
```

At the bottom:

```
[[ $- != *i* ]] && return # Stop here if not running interactively
[[ $(hostname) = "jasmin-cylc.ceda.ac.uk" ]] && . mosrs-setup-gpg-agent
# Enable bash completion for Rose commands
[[ -f /apps/contrib/metomi/rose/etc/rose-bash-completion ]] && . /apps/contrib/metomi/rose/
etc/rose-bash-completion
```

Now, whenever login to jasmin-cylc you should be prompted for your Met Office Science Repository Service password.

A further setup for JASMIN and MOSRS requires an update to your ~/.subversion/servers file. Please add the following and do not forget to give the corresponding username (change **myusername** word for your **MOSRS-username**).

```
[groups]
metofficesharedrepos = code*.metoffice.gov.uk

[metofficesharedrepos]
# Specify your Science Repository Service user name here
username = myusername
store-plaintext-passwords = no
```

In the ~/.subversion/config file comment any lines starting with:

```
#password-stores =
```

Create the following configuration file ~/.metomi/fcm/keyword.cfg and add the following lines:

```
location{primary, type:svn}[jules.x]=https://code.metoffice.gov.uk/svn/jules/main
browser.loc-tmpl[jules.x]=https://code.metoffice.gov.uk/trac/{1}/intertrac/source:/{2}{3}
browser.comp-pat[jules.x]=(?msx-i:\A // [^/]+ /svn/ ([^/]+) /*(.*) \z)

location{primary, type:svn}[jules_doc.x]=https://code.metoffice.gov.uk/svn/jules/doc
browser.loc-
tmpl[jules_doc.x]=https://code.metoffice.gov.uk/trac/{1}/intertrac/source:/{2}{3}
browser.comp-pat[jules_doc.x]=(?msx-i:\A // [^/]+ /svn/ ([^/]+) /*(.*) \z)
```

Add the following lines on the ~/.metomi/rose.conf file if missing (change **myusername** word for your **MOSRS-username**):

```
[rosie-id]
prefix-default=u
prefix-location.u=https://code.metoffice.gov.uk/svn/roses-u
prefix-username.u=myusername
#username is all in lower case
prefix-ws.u=https://code.metoffice.gov.uk/rosie/u

[rose-stem]
automatic-options=SITE=jasmin
```

This can be checked by running:

```
rose config
```

Appendix B: Plant Functional Type, Leaf Area Index and Canopy Height Cross-Walking Tables

Table B1. PFT fraction lookup table for vegetated PFTs only. BLT = Broadleaf Tree; NLT = Needleleaf Tree. These lookup tables are used in conjunction with equations 1 and 2.

	BLT	NLT	C3 Grass	C4 Grass	Shrub	Urban	Water	Bare Soil	Ice
Evergreen Needleleaf forest	0	70	20	0	0	0	0	10	0
Evergreen Broadleaf forest	85	0	0	10	0	0	0	5	0
Deciduous Needleleaf forest	0	65	25	0	0	0	0	10	0
Deciduous Broadleaf forest	60	0	5	10	5	0	0	20	0
Mixed forest	35	35	20	0	0	0	0	10	0
Closed shrub	0	0	25	0	60	0	0	15	0
Open shrub	0	0	5	10	35	0	0	50	0
Woody savannah	50	0	15	0	25	0	0	10	0
Savannah	20	0	0	75	0	0	0	5	0
Grassland	0	0	70	15	5	0	0	10	0
Permanent wetland	0	0	80	0	0	0	20	0	0
Cropland	0	0	75	5	0	0	0	20	0
Urban	0	0	0	0	0	100	0	0	0
Crop/natural mosaic	5	5	55	15	10	0	0	10	0
Snow and ice	0	0	0	0	0	0	0	0	100
Barren	0	0	0	0	0	0	0	100	0
Water bodies	0	0	0	0	0	0	100	0	0

5 **Table ~~5~~B2. Leaf Area Index lookup table for combinations of IGBP land cover class and plant functional type. These lookup tables are used in conjunction with equations 1 and 2.**

	Broadleaf Tree	Needleleaf Tree	C3 Grass	C4 Grass	Shrub
Evergreen Needleleaf forest		6	2		
Evergreen Broadleaf forest	9		2	4	
Deciduous Needleleaf forest		4	2		
Deciduous Broadleaf forest	5		2	4	3
Mixed forest	5	6	2		

Closed shrub			2		3
Open shrub	5		2	4	2
Woody savannah	9		4		2
Savannah	9			4	
Grassland			3	4	3
Permanent wetland	9		3		3
Cropland	5		5	4	3
Urban					
Crop/natural mosaic	5	6	4	4	3
Snow and ice					
Barren					
Water bodies					

Table B3. PFT-dependent canopy height scaling factor

	Broadleaf Tree	Needleleaf Tree	C3 Grass	C4 Grass	Shrub
Canopy height factor	6.5	6.5	0.5	0.5	1.0

---

i